



Rat atrial engineered heart tissue: a new in vitro model to study atrial biology

Julia Krause^{1,2} · Alexandra Löser^{2,3} · Marc D. Lemoine^{2,3,4} · Torsten Christ^{2,3} · Katharina Scherschel^{2,4} · Christian Meyer^{2,4} · Stefan Blankenberg^{1,2} · Tanja Zeller^{1,2} · Thomas Eschenhagen^{2,3} · Justus Stenzig^{2,3}

Received: 19 February 2018 / Accepted: 27 August 2018 / Published online: 3 September 2018
© Springer-Verlag GmbH Germany, part of Springer Nature 2018

Abstract

Engineered heart tissue (EHT) from rat cells is a useful tool to study ventricular biology and cardiac drug safety. Since atrial and ventricular cells differ significantly, EHT and other 3D cell culture formats generated from ventricular cells have been of limited value to study atrial biology. To date, reliable in vitro models that reflect atrial physiology are lacking. Therefore, we established a novel EHT model using rat atrial cells (atrial EHT, aEHT) to assess atrial physiology, contractility and drug response. The tissue constructs were characterized with regard to gene expression, histology, electrophysiology, and the response to atrial-specific drugs. We observed typical functional properties of atrial tissue in our model such as more regular spontaneous beating with lower force, shorter action potential duration, and faster contraction and relaxation compared to ventricular EHT (vEHT). The expression of atrial-specific genes and proteins was high, whereas ventricle-specific transcripts were virtually absent. The atrial-selective drug carbachol had a strong negative inotropic and chronotropic effect on aEHT only. Taken together, the results demonstrate the feasibility of aEHT as a novel atrial 3D model and as a benchmark for tissue engineering with human induced pluripotent stem cell-derived atrial-like cardiomyocytes. Atrial EHT faithfully recapitulates atrial physiology and shall be useful to study atrial molecular physiology in health and disease as well as drug response.

Keywords Atrial fibrillation · Tissue engineering · Electrophysiology · Drug screening

Julia Krause and Alexandra Löser contributed equally.

Electronic supplementary material The online version of this article (<https://doi.org/10.1007/s00395-018-0701-2>) contains supplementary material, which is available to authorized users.

✉ Justus Stenzig
j.stenzig@uke.de

¹ Department of General and Interventional Cardiology, University Heart Center Hamburg, Martinistrasse 52, 20246 Hamburg, Germany

² DZHK (German Centre for Cardiovascular Research), Partner site Hamburg/Kiel/Lübeck, Hamburg, Germany

³ Department of Experimental Pharmacology and Toxicology, University Medical Center Hamburg-Eppendorf, Martinistrasse 52, 20246 Hamburg, Germany

⁴ Department of Cardiology-Electrophysiology, University Heart Center Hamburg, Martinistrasse 52, 20246 Hamburg, Germany

Introduction

Cardiovascular disease (CVD) represents the leading cause of death worldwide. One common CVD is atrial fibrillation (AF), the most frequent sustained rhythm disorder [31]. AF is often asymptomatic but is associated with increased risk of stroke and heart failure [28]. The mechanisms underlying AF are still incompletely understood and include a wide range of concepts from ion channel modulation, inflammation, and atrial fibrosis to deregulation of cardiac developmental pathways [2, 36]. The rising incidence of AF with age and the aging population leads to an increasing prevalence of AF, emphasizing the need for a deeper understanding of the pathomechanisms [23, 33]. This may have important implications with respect to diagnosis and the identification of novel therapies.

Over the last decades, engineered three-dimensional cardiac-like tissue constructs have been developed, which combine some of the advantages of both animal models and 2D cell culture [15]. Force developing 3D tissue constructs provide the same degree of standardization and

reproducibility as 2D cell culture. At the same time, they mimic part of the multicellular architecture of the native heart and importantly allow for contractility analysis [39]. Numerous studies demonstrated that engineered heart tissue (EHT) from rat cells can be successfully used as a tool to study ventricular biology and as a screening platform for cardiac drug safety [8, 10, 13, 17, 39]. Screening for cardiotoxicity, in particular, is often restricted in animal models. Novel drugs and broader concentration ranges of potentially toxic substances can be systematically assessed without ethical concerns in rat EHT.

However, ventricular EHT (vEHT) does not reflect the complexity of the heart in terms of the atrial and ventricular cardiomyocyte phenotype. The striking functional and molecular differences between atrial and ventricular cardiomyocytes emphasize the need for atrial *in vitro* models [3, 27].

Therefore, we set out to establish and characterize a 3D model using rat atrial cells. We analyzed our model with regard to gene expression, histology, contractility, electrophysiology, and drug response (Fig. 1). Results were directly compared to parallel experiments with vEHT and to atrial and ventricular heart muscle preparations from adult rats.

Materials and methods

Generation of aEHT and vEHT (find a detailed protocol in the supplement)

All animal work was conducted in accordance with the Guide for the Care and Use of Laboratory Animals as adopted by the United States National Institutes of Health (NIH publication no. 85-23, revised 1996) and was approved by the local Animal Welfare Committee of the City of Hamburg, Germany (approval #08/14). Ventricular EHT was prepared according to previously described protocols in a 24-well cell culture format [13]. Atrial EHT was prepared in a similar way. A detailed step-by-step protocol can be found in the supplement. In brief, the atria and ventricles from neonatal Wistar rats (postnatal day 0–3) were mechanically separated at the valve plane and separately exposed to repeated DNase and trypsin digestion. For preparation of a single EHT, 625,000 atrial or ventricular heart cells were mixed with fibrinogen, thrombin and DMEM. The mix was pipetted into an agarose casting mold between the two flexible silicone posts of a silicone rack, on which up to four EHTs were cultured simultaneously. After a 1.5 h incubation time, during which the fibrinogen solidified to form

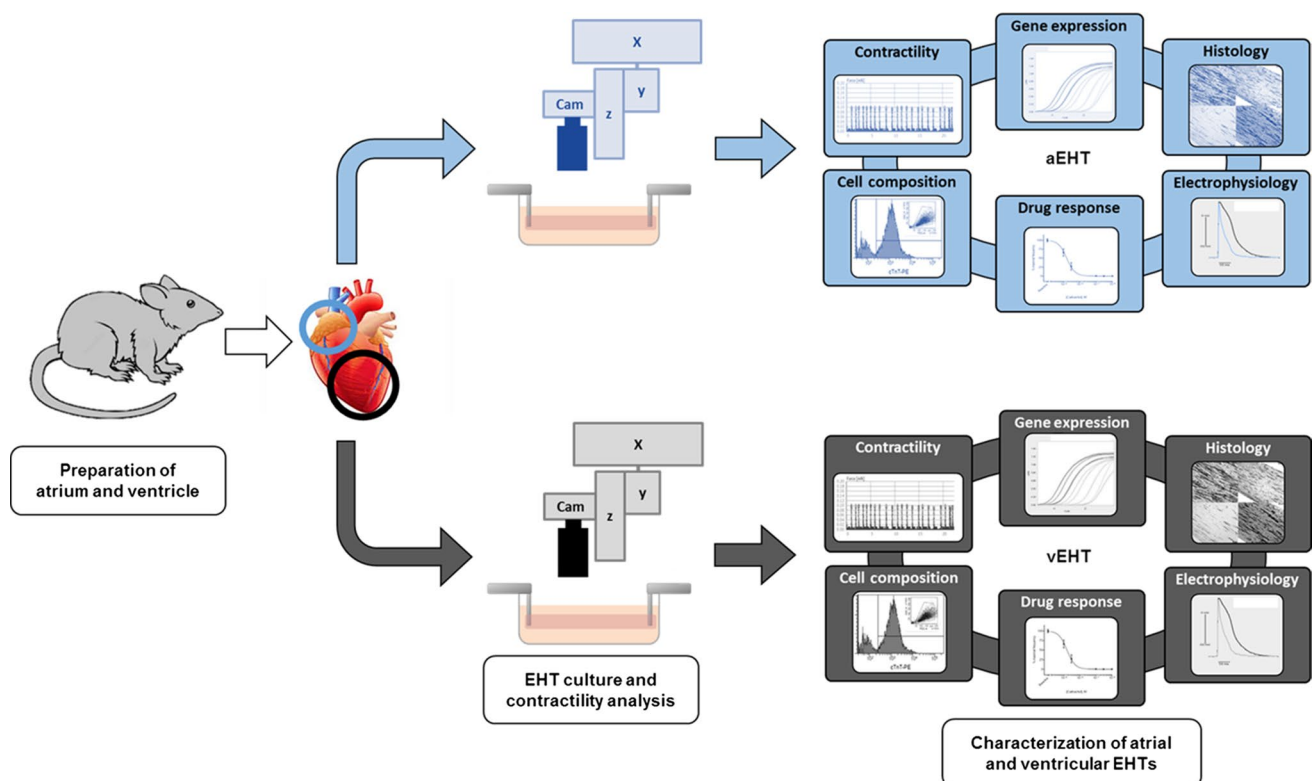


Fig. 1 Experimental outline. We have established a novel EHT model using rat atrial cells. Both aEHT and already established vEHT were characterized with regard to contractility, gene expression, histology, cell composition, electrophysiology, and the response to atrial-acting drugs

the extracellular matrix, the EHTs were transferred to a cell culture dish containing EHT medium (DMEM, 10% horse serum inactivated, 1% penicillin/streptomycin, 10 µg/mL insulin, 33 µg/mL aprotinin). The EHTs were cultured in a 37 °C, 7% CO₂, and 40% O₂ humidified cell culture incubator. Medium change was performed three times per week. The EHTs were treated with 25 µM of the mitosis inhibitor 1-beta-D-arabinofuranosylcytosine (AraC) either once after casting for 48 h or once per week.

Video-optical recordings

Analysis of contractile parameters was performed as described before [13]. In brief, the 24-well cell culture plates containing the EHTs were transferred to a custom-designed glass roof-incubator with controlled atmosphere, temperature, and humidity, which was coupled to a three-dimensionally movable camera and pattern recognition software. Deflection of the posts by the EHTs was optically recorded and used to calculate the contractile parameters with a customized software (CTMV, Pforzheim, Germany).

Electrical pacing

Short-term pacing of EHTs under video-optical recording was performed as described before [16] with custom-made graphite-based pacing units onto which the EHT racks were mounted. Biphasic pacing pulses of 4 ms were applied (Grass S88X Dual Output Square stimulator, Natus Neurology Incorporated) at 2 V.

Analysis of contractile force in primary rat tissue

Contraction measurements in primary rat tissues were performed as described before [5]. In short, spontaneously beating left atria and left ventricular papillary muscles were isolated from 10 to 12 weeks old male Wistar rats and transferred to Swema 4–45 strain gauge transducers in modified Tyrode's solution (in mM: NaCl 126.9, KCl 5.4, CaCl₂ 1.8, MgCl₂ 1.05, NaHCO₃ 22, NaH₂PO₄ 0.45, EDTA 0.04, ascorbic acid 0.2, pyruvate 5 and glucose 5.0; pH 7.4) at 37 °C. Tissues were paced at 2 Hz and stretched. Force recordings were performed with PowerLab amplifiers on a Chart for Windows, version 5.0 recording program (ADInstruments). Time to peak force and to half-maximal relaxation were calculated using ChartPro for Windows version 5.51 analysis program (ADInstruments).

Flow cytometry

The proportion of cardiomyocytes among the isolated rat cells was determined by flow cytometry both after atrial and ventricular cell preparation. To this end, the cells underwent

a live/dead staining (Fixable Viability Dye eFluor 450, eBioscience #65-0863-14), followed by fixation with Histofix for 20 min (Roth #A146) and permeabilization in PBS containing 5% FCS, 0.5% Saponin, and 0.05% sodium azide for 1 h at 4 °C. Staining was carried out with a PE-labeled antibody directed against cardiac troponin T (cTnT, Miltenyi, #130-106-688) 1:100 in permeabilization buffer for 1 h at 4 °C. Flow cytometric analysis was done on a BD FACSCanto II flow cytometer (BD Biosciences).

Gene expression analysis

Total RNA was isolated from freshly prepared cardiac cells or homogenized EHT (QIAGEN TissueLyser) at different time points during culture with the RNeasy Plus Mini Kit (Qiagen) and converted to cDNA with the High-Capacity cDNA Reverse Transcription Kit (Applied Biosystems). Relative transcript levels of atrial and ventricular markers were analyzed with the 5×HOT FIREPol EvaGreen qPCR Mix Plus ROX (Solis BioDyne) on an ABI PRISM 7900HT Sequence Detection System qPCR cyclers (Applied Biosystems). The primer sequences for each analyzed target are shown in supplementary table S1. Glucuronidase beta (*Gusb*) was used as a housekeeping gene for normalization and calculation of relative expression with the $\Delta\Delta\text{CT}$ -method.

Histology

At the end of culture, the EHTs were fixed overnight with 4% formaldehyde and embedded in paraffin. Longitudinal sections of 4 µm were produced for hematoxylin and eosin (H&E) staining and immunohistochemical staining. H&E staining was performed in an automated manner according to the standard procedure. Immunohistochemical staining including deparaffinization and antigen retrieval was carried out on the BenchMark XT system (Ventana). Antigen retrieval was done by 30-min incubation with citrate buffer. Optimized antibody concentrations were: Mlc2a (Synaptic Systems, SY 311 011) 1:75, Mlc2v (Synaptic Systems, SY 310 111) 1:150, alpha-actin (Dako M 0874) 1:200, vimentin (Dako, M0725) 1:200. Antibody visualization was performed with the UltraView Universal DAB Detection Kit (Roche, #05269806001) and microscopic imaging was carried out on an AxioScope 2 microscope (Zeiss). The vimentin-positive cells were counted in a semi-automatic manner using Image J software [30].

Immunohistochemistry

Whole-mount immunostaining of vEHT and aEHT was performed as described previously [18]. In short, EHTs were fixed with 4% formaldehyde and permeabilized with 0.25% Triton/phosphate buffered saline (PBS). Next, EHTs were

treated with 0.25% Sudan Black in 70% ethanol for reduction of autofluorescence and blocked overnight with BSA. Incubation with primary (mouse anti-troponin T, Dianova #dln-008802, 1:1) and secondary (donkey anti-mouse 647, Life Technologies A-31571, 1:500) antibodies was performed at 4 °C for 48 and 12 h, respectively. EHTs were embedded in DAPI Fluoromount-G (Southern Biotech) and analyzed with a Leica TCS SP2 imaging system (Leica Microsystems).

Carbachol drug testing

Drug testing was regularly performed 1 day after media change. Fresh serum-free DMEM (Biochrom F04115) containing 10 mM HEPES was pre-incubated on the morning of the experiment at 37 °C, 40% O₂, 7% CO₂, and 90% humidity for 2 h. The aEHTs and vEHTs were transferred into the DMEM and incubated for 45 min. After measurement of basal activity in DMEM (pre-baseline), for frequency measurements only, 50 nM epinephrine was added to each well to enhance likelihood of contraction within the recording time and the baseline was measured. The EHTs were then exposed to increasing concentrations of carbachol (10 nM, 30 nM, 100 nM, 300 nM, 1 μM, 10 μM, plus 50 nM of epinephrine for frequency measurements) and response to each concentration was measured with the video-optical recording system. The described experiments were performed both with and without electrical stimulation. Electrical pacing was performed using custom-made graphite-based pacing electrodes as described before, with biphasic pulses of 4 ms per polarity, 2 V and 1.5 Hz [16].

Electrophysiology

Action potentials (APs) were recorded with standard sharp microelectrodes in intact aEHT or vEHT (14–21 days old), superfused with Tyrode's solution at 36.5 ± 0.5 °C, field stimulated at 1 Hz (n = number of total impalements, vEHT n = 12, aEHT n = 8 [21, 22]). Bath solution contained (in mM): NaCl 127, KCl 5.4, MgCl₂ 1.05, CaCl₂ 1.8, Glucose 10, NaHCO₃ 22, NaHPO₄ 0.42, equilibrated with O₂:CO₂ [95:5] at 36.5 ± 0.5 °C, pH 7.4. APs were analyzed offline using the Lab-Chart software (ADInstruments).

Results

Establishment of the aEHT model

We aimed to establish an atrial EHT model made from neonatal rat heart cells and based our work on published protocols for the generation of vEHT [13]. The final protocol

for atrial cell isolation and the generation of fibrin-based aEHT is provided as a step-by-step instruction in the supplement (see suppl. S5 & S6). After the isolation of atrial and ventricular cells by trypsin/DNase digestion, viability and cardiomyocyte fraction were analyzed by flow cytometry (cardiac troponin T staining). Both atrial and ventricular cell isolations resulted in ~85% viable cells, out of which more than ~75% stained positive for the cardiomyocyte marker troponin T (Fig. S1, a and b).

Culture of aEHT only slightly differed from published vEHT culture. The excessive proliferation of non-myocytes in aEHT led to typical shortening of EHTs (Fig. S1c), necessitating treatment with 1-beta-D-arabinofuranosylcytosine (AraC), an inhibitor of DNA polymerase alpha and beta, as published for mouse EHT [34]. We evaluated one-time and weekly treatment. Compared to a one-time treatment after 2–3 days of cultivation, the weekly supplementation prolonged the period of stable contractile performance of the aEHT to at least 3 weeks (Fig. S1, d and e). This was also reflected on the level of fibroblast marker gene expression, which were higher in EHTs receiving the one-time treatment with AraC only, compared to weekly treatment (Fig. S1f). We did not observe an acute effect of the treatment on contractility, gene expression or histology. For better comparability, vEHTs were treated in the same way.

For clarity of the representation of results, data from several batches of aEHT were pooled. Exemplarily, a separate analysis of each batch of EHTs can be found for day 14–15 in the supplement (Fig. S4) and illustrates low batch-to-batch variability.

Development and morphology

Compared to vEHT, development of aEHT was faster and reached the plateau stage of stable contractile force earlier (Fig. 2). First twitching of single cells was already detected at day 3 after casting, which is usually only observed on day 5 in vEHT. Coherent beating started after 4 (aEHT) and 6 days of culture (vEHT), respectively. Force generation of aEHT reached a plateau after 9 days, whereas in vEHT, force increased until day 10. Both types of EHT could be stably cultured for more than 30 days. To assess remodeling and structural organization, we analyzed H&E-stained paraffin sections of aEHT and vEHT at the end of culture (day 30). Both models displayed a network of longitudinally aligned cells, which were mostly homogeneously distributed inside the tissue with some accumulation near the surface of the construct, as has been described before ([13], Fig. S2, a and b). Staining for α-actin revealed the expected cross-striated pattern in cardiomyocytes, shown for aEHT in Fig. S2, c and d.

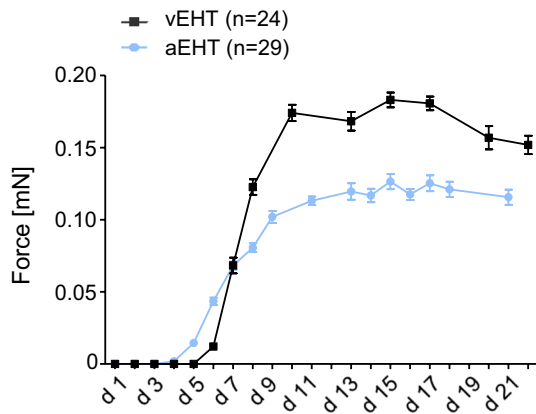


Fig. 2 Force development of vEHT and aEHT. Force generation of aEHT reached a plateau phase earlier (day 9) than vEHT (day 10). Error bars display SEM

Contractile properties

Contractility of all EHTs was analyzed regularly by video-optical recording. Despite the similar morphology, we observed significant differences in the beating pattern of

the two models. While vEHT beats in bursts interrupted by periods of inactivity ([16], Fig. 3a, b), aEHT displayed continuous and more regular beating. In addition, the spontaneous beating frequency of aEHT was significantly lower than in vEHT (59.0 ± 1.6 bpm, $n = 124$ vs. 90.3 ± 4.1 bpm, $n = 207$, respectively; Fig. 4a). During the plateau phase of stable contractile force (day 14–15), vEHT developed a $1.3 \times$ higher average force than aEHT despite the same number of cells per tissue (0.17 ± 0.003 mN, $n = 231$ and 0.13 ± 0.003 mN, $n = 124$, respectively; Fig. 4b). Moreover, the contraction and relaxation kinetics were significantly faster in aEHT, displaying a 49% lower contraction time (T1, time from 20% above baseline to maximum force) and a 53% lower relaxation time (T2, time from peak back to 20% above baseline, Fig. 4c, d). Normalized average contraction peaks for both atrial and ventricular EHTs were compared to measurements from adult rat left ventricular and atrial tissue (Fig. 5a). Even though EHT in general was significantly slower than native tissue, with regard to time to peak and time to 50% relaxation, the overall shape of the peaks and the relation between aEHT and vEHT were identical to adult tissue (Fig. 5b).

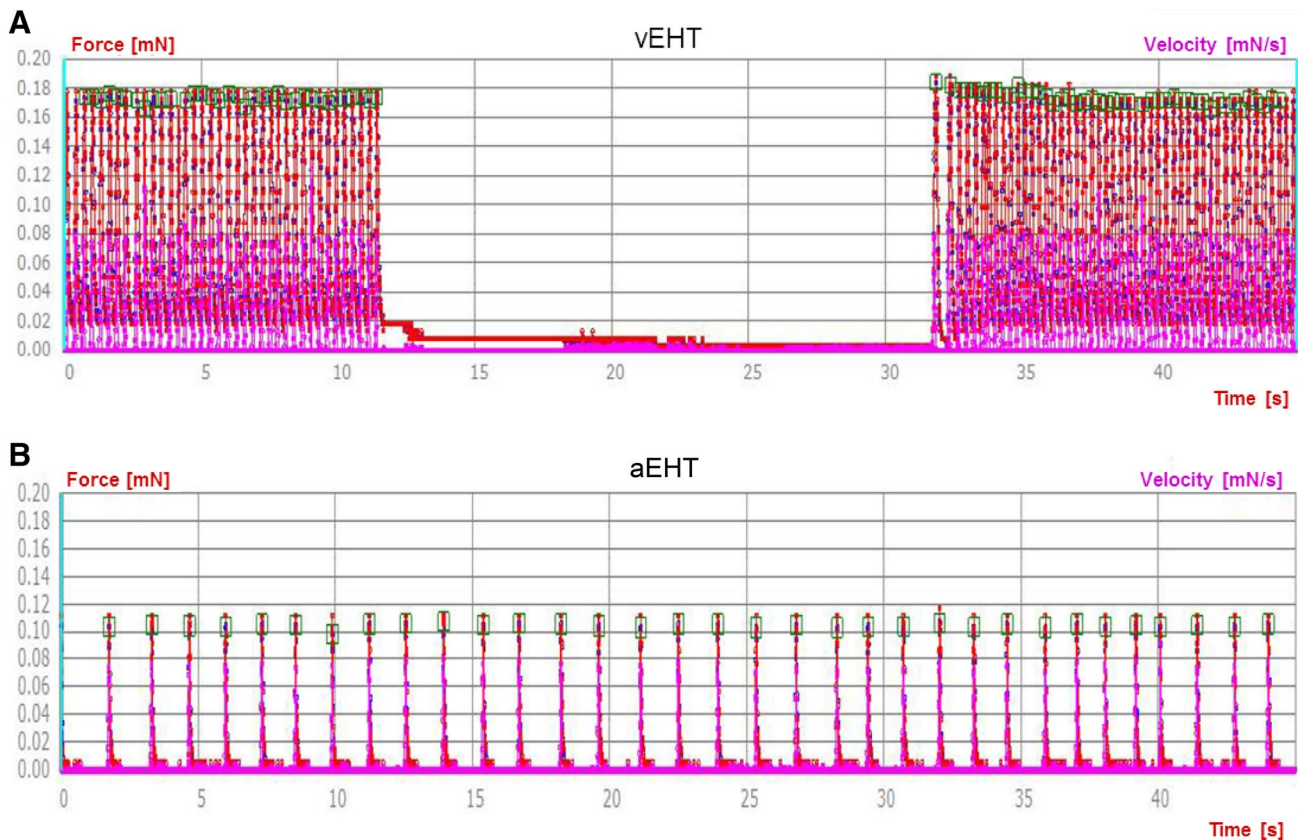


Fig. 3 Beating pattern of vEHT and aEHT. **a** vEHT beats in bursts, interrupted by periods of inactivity whereas **b** aEHT beats in a regular manner. **a, b** Show representative traces from the EHT analysis software (CTMV, EHT Technologies GmbH)

Fig. 4 Spontaneous contractility of vEHT and aEHT (day 14–15). Video-optical analysis of **a** spontaneous beating frequency, **b** force, **c** contraction time (T1, from 20% to peak) and **d** relaxation time (T2, from peak to 20%) in aEHT and vEHT. Bars show mean \pm SEM, unpaired *t* test, ****p* < 0.001, all numbers refer to total number of EHTs/number of batches

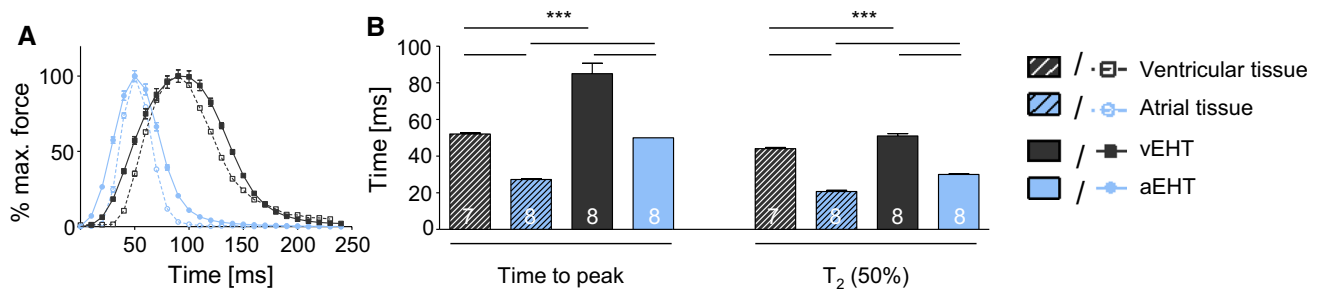
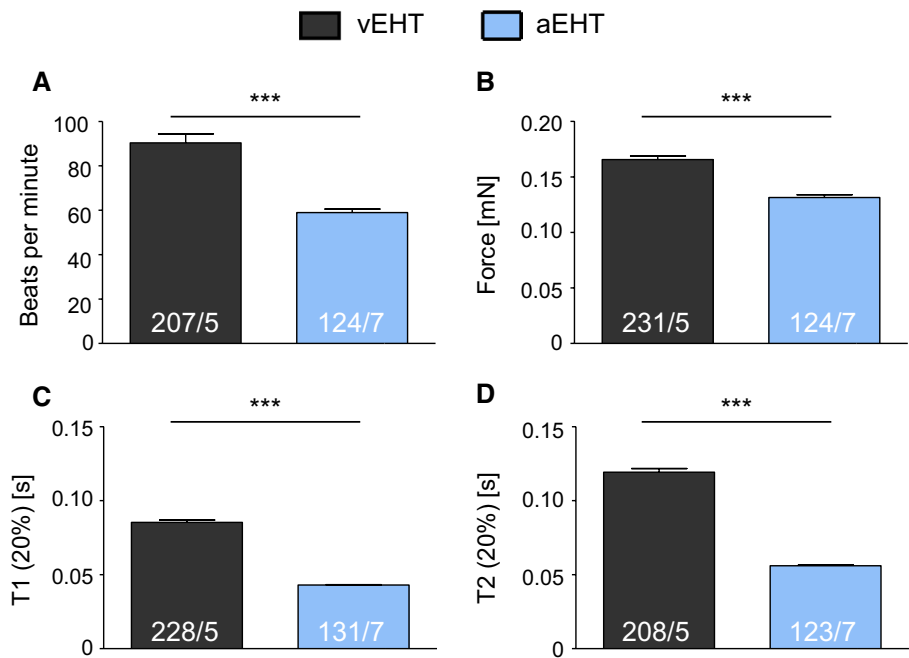


Fig. 5 Contraction peaks under pacing. **a** Normalized average contraction peaks of 60 individual peaks for both aEHT and vEHT compared to adult rat left ventricular and atrial tissue. **b** Time to peak (time from pacing pulse to peak) and time to 50% relaxation for

both EHT models and tissue samples. Error bars show mean \pm SEM, One-way ANOVA, Bonferroni post-test for multiple comparisons, ****p* < 0.001

Action potential duration and force–frequency relationship

An important difference between atrial and ventricular cardiomyocytes is the shorter action potential duration (APD) in atrial cells [1]. To test whether our EHT models mirror this electrophysiological property, we performed sharp microelectrode action potential measurements on intact EHTs. Again, we used atrial and ventricular tissue samples from adult rat for comprehensive comparison. APD measurements in adult tissue samples, as expected, revealed a 47% shorter APD₉₀ in atrial compared to ventricular tissue (29.0 \pm 3.0 ms, *n* = 5 and 54.5 \pm 3.9 ms, *n* = 7 per group; Fig. 6a). The absolute values for the APD₉₀ in atrial and ventricular EHTs were 1.24 and 1.57 times higher compared to the tissue (74.6 \pm 11.9 ms, *n* = 8 and 121.9 \pm 3.2 ms, *n* = 12,

respectively; Fig. 6c). However, the ratio between atrial and ventricular EHT APD₉₀ was similar to that of adult tissue, revealing an approximately 40% shorter AP in atrial EHTs (Fig. 6b). In order to analyze whether different ion channel remodeling in vitro was underlying the observed differences between EHT and adult tissue, we performed gene expression analysis of ion channel subunits on day 1 and day 30 of EHT culture and compared the results to adult tissue (Fig. 6d–g). We observed an upregulation for all analyzed channels in EHT over time. On day 30, expression of *Cacna1c*, *Kcnd3*, and *Kcnh2* was in the range of the levels in the respective native tissues. However, *Kcnj2* displayed a lower expression in vEHT compared to ventricular tissue.

To evaluate the physiological implications of our findings, we analyzed the force–frequency relationship (FFR)

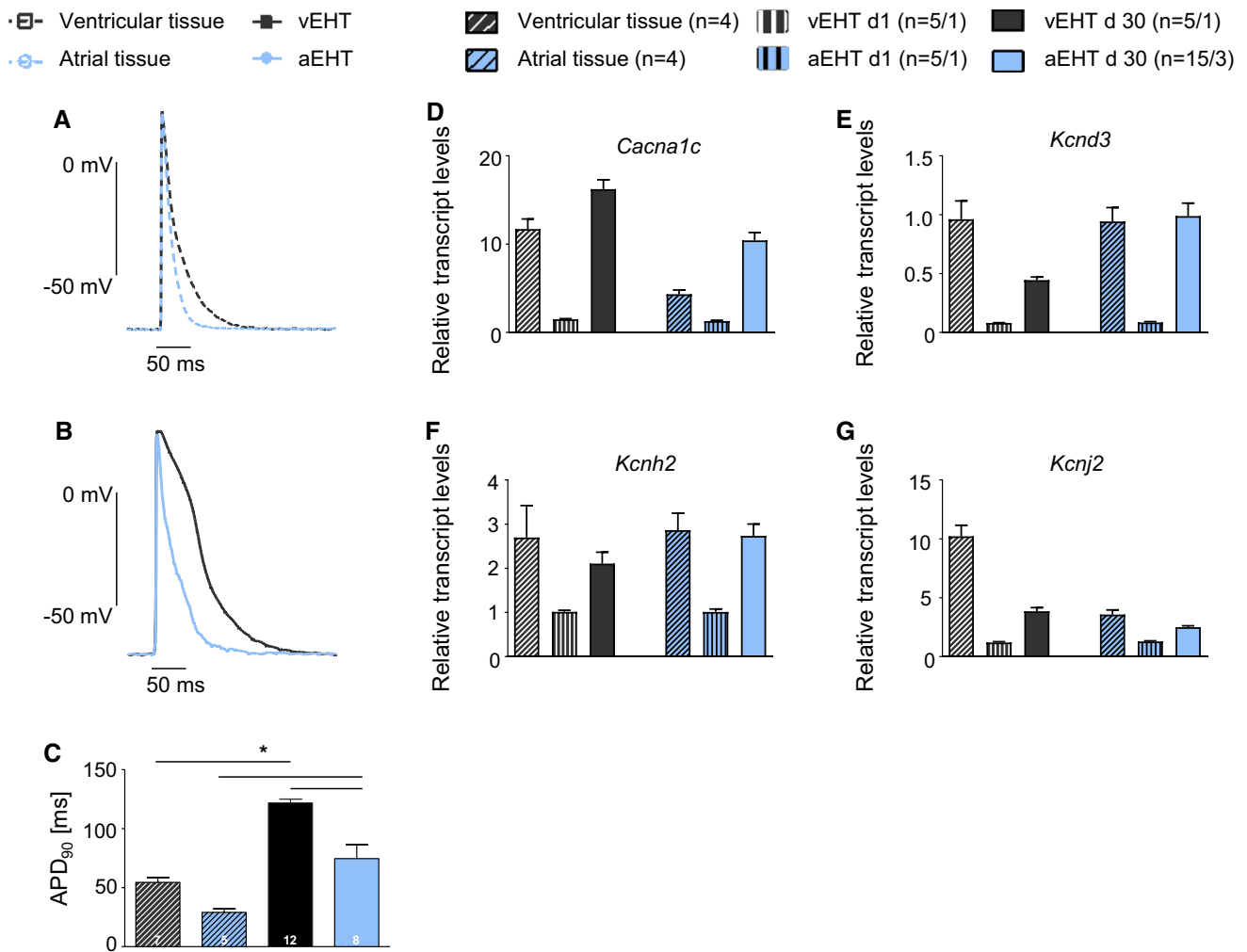


Fig. 6 Action potentials. Representative action potentials of **a** atrial and ventricular adult rat tissue and **b** aEHT and vEHT on day 14–21 at 1 Hz. **c** Action potential duration (APD) at 90% repolarization for tissues and EHT models. Ion channel remodeling of *Cacna1c* (**d**),

Kcnd3 (**e**), *Kcnh2* (**f**), and *Kcnj2* (**g**) was analyzed by qPCR on day 1 and day 30 and compared to adult tissues. Mean ± SEM, One-way ANOVA, Bonferroni post-test for multiple comparisons, **p* < 0.05

of our two EHT models, which is known to be affected by the duration of the action potential. For this purpose, the EHTs were electrically paced with increasing frequencies (1–10 Hz). Atrial EHT was able to follow the pacing pulses up to the highest frequency, while vEHT started to lose pacing capture at frequencies of 6 Hz or higher (Fig. 7a, b). In both models, we observed a decrease in force with increasing frequencies (negative FFR). This decline in force was significantly more pronounced and started at lower frequencies in vEHT (Fig. 7c). Moreover, while the relaxation time of vEHT decreased with increasing frequencies [frequency-dependent acceleration of relaxation (FDAR)], the contraction peaks of atrial EHTs remained stable independently of pacing frequency (Fig. 8a through c).

Gene expression and histology

To confirm the atrial identity of the cardiomyocytes in our aEHT model, we analyzed the expression of genes with known differential expression in atrial and ventricular cardiomyocytes, including transcription factors, structural proteins and ion channels (Table S2). For comparison and as control, we additionally analyzed vEHTs, as well as adult rat atrial and ventricular tissue samples. All markers displayed the expected tissue distribution. This is exemplified by the transcript levels of the ventricular and atrial isoforms of the myosin regulatory light chain (*My12* and *My17*, respectively; Fig. 9a, b). Both genes revealed a similar ratio of relative transcript levels between aEHT and vEHT as observed in the adult tissue samples. *Kcnj3*, encoding the potassium channel GIRK1, which generates the atrial and nodal-specific

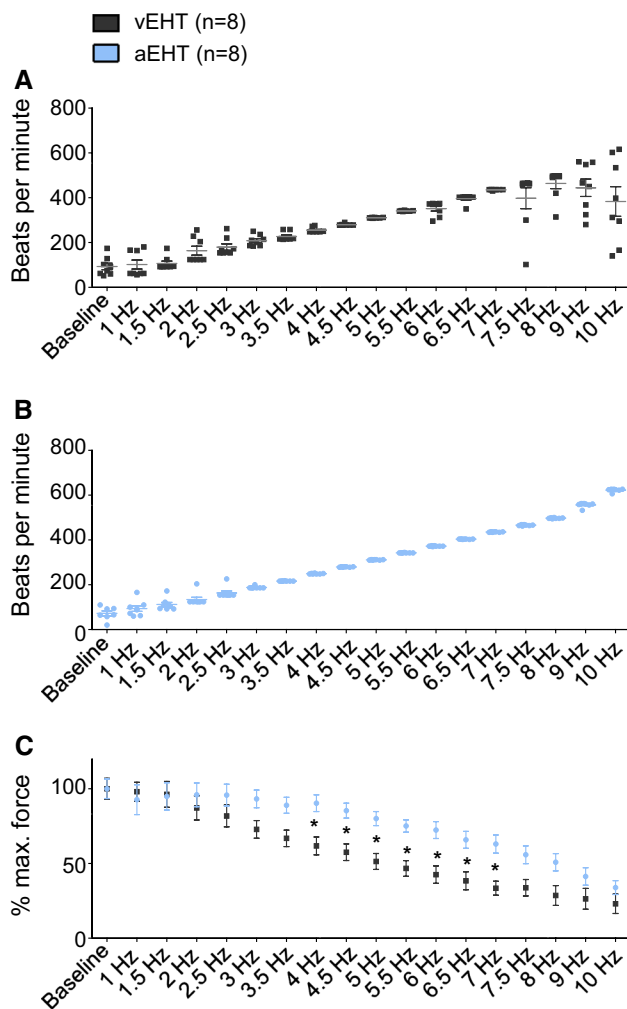


Fig. 7 Force–frequency relationship (FFR). vEHT and aEHT were electrically paced with increasing frequencies (1–10 Hz) at day 23. Beating frequencies under electrical stimulation of **a** vEHT and **b** aEHT. **c** Force development of aEHT and vEHT at different frequencies. Mean \pm SEM, Two-way ANOVA, Bonferroni post-test for multiple comparisons, * $p < 0.05$

$I_{K_{ACH}}$ current (Fig. 9c), displayed a similar expression pattern. Additionally, two markers for pacemaker cells, *Thyl* and *Shox2*, were analyzed. Both were significantly higher expressed in aEHT, while the expression in vEHT was comparatively low (Fig. S3, k and l). The expression of the remaining analyzed genes is displayed in supplementary Fig. S3.

To evaluate our findings on protein level, we performed immuno-histological staining for the myosin regulatory light chain isoforms Mlc2a and Mlc2v. The main isoform in aEHT was indeed Mlc2a (Fig. 9a, b), while only a few cells stained positive for the ventricular isoform. As expected, vEHT displayed an inverted staining pattern with most of the cells only Mlc2v positive. Furthermore, we performed whole-mount staining of EHTs for cardiac troponin T (Fig. 9d, e).

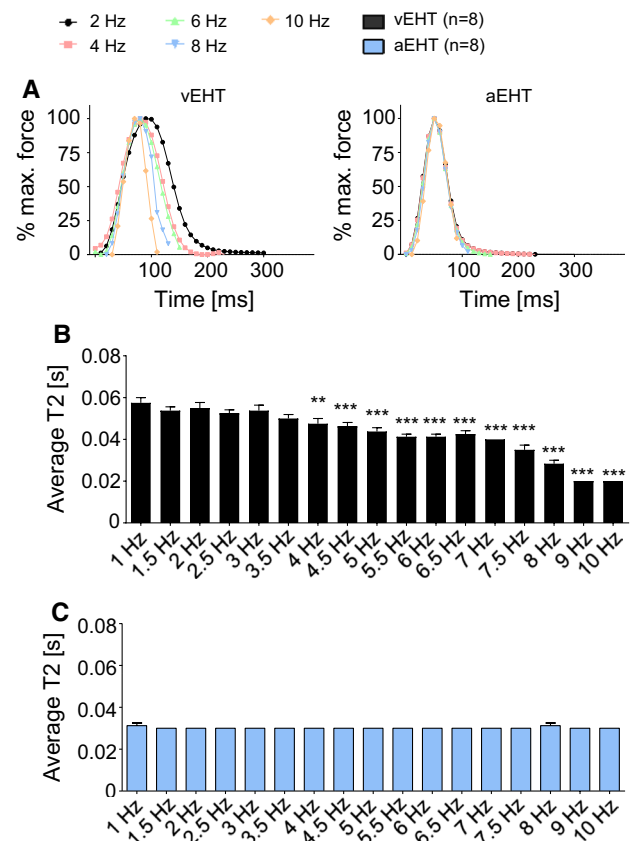


Fig. 8 Frequency-dependent acceleration of relaxation (FDAR). **a** Normalized contraction peaks of both models at different pacing frequencies. Average relaxation time at different pacing frequencies for **b** vEHT and **c** aEHT. Bipolar electrical stimulation at 2 V and 4 ms pulse duration. Mean \pm SEM, One-way ANOVA, Dunnett's post-test to control (1 Hz) ** $p < 0.005$, *** $p < 0.001$

For both models, we observed the expected striation and the longitudinal alignment. In addition, the atrial cardiomyocytes were thinner than their ventricular counterparts as has been described before [32]. To further elucidate the composition of types of EHT with regard to their fibroblast content, we performed vimentin staining on day 1 and day 30 of EHT culture (Fig. 10). Both groups showed the same proportion of vimentin-positive cells at both time points, suggesting successful suppression of cell proliferation with the mitosis inhibitor AraC.

Effect of muscarinic stimulation by carbachol

To further validate our EHTs as an atrial model, we challenged them with the cholinomimetic drug carbachol, which activates the atrial and nodal-specific repolarizing potassium current $I_{K_{ACH}}$ by binding to the muscarinic acetylcholine receptor M_2 . Ventricular EHT was treated in parallel and served as control. Figure 11a shows concentration–response curves for aEHT and vEHT with respect to contractility. We observed a

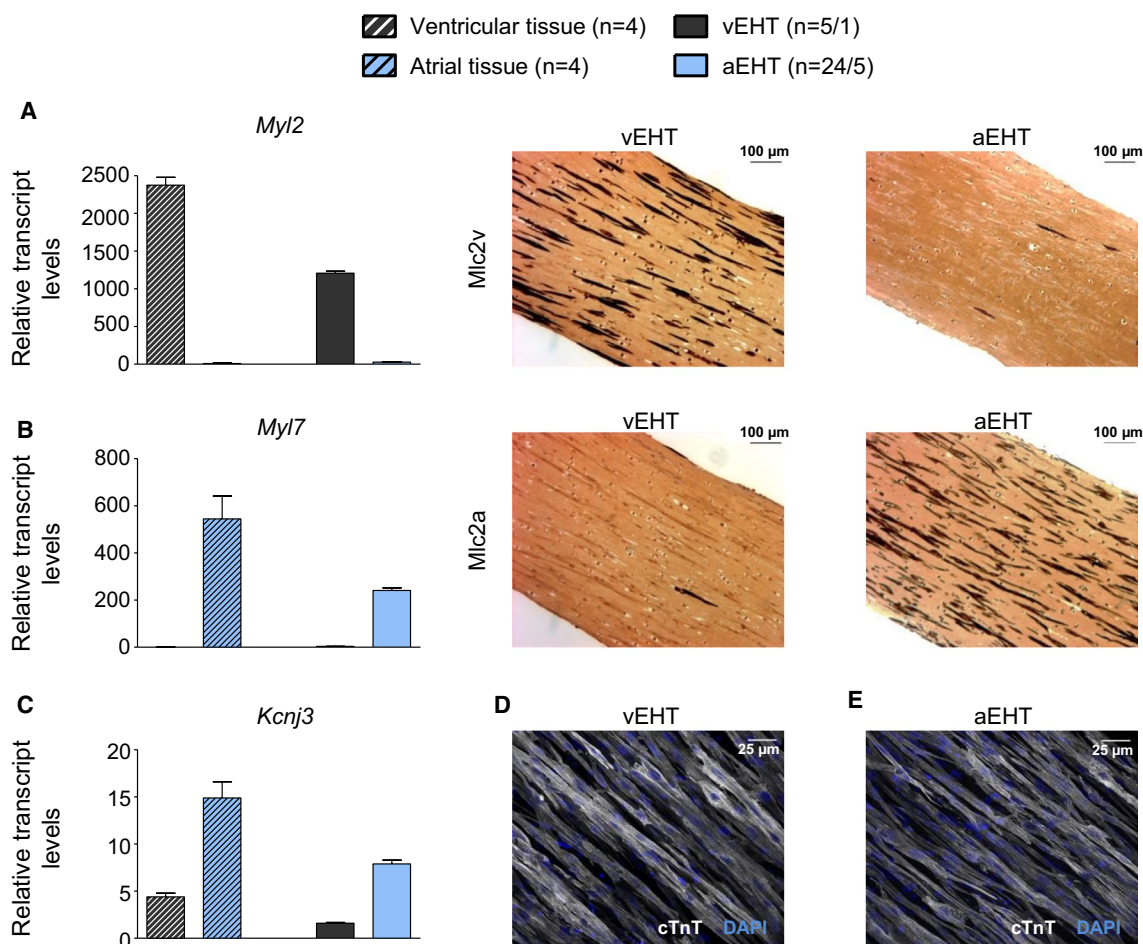


Fig. 9 Gene expression and histological analysis. Gene expression analysis was performed in 30 days-old EHTs and compared to adult rat tissue samples from atrium and ventricle. **a, b** Relative transcript levels of the ventricular and atrial isoforms of the myosin regulatory light chain (*Myl2* and *Myl7*) compared to adult tissue samples with corresponding *Mlc2v* and *Mlc2a*-stained paraffin sections of aEHT

and vEHT. **c** Relative transcript levels of the atrial-specific *Kcnj3* gene. **d, e** Confocal microscopic images of whole-mount staining of cardiac troponin T in vEHT and aEHT, respectively (white), nuclei counter-stained with DAPI (blue). Transcript levels were normalized to the housekeeping gene *Gusb*. Error bars show mean \pm SEM

concentration-dependent negative chronotropic effect in both aEHT and vEHT (in the presence of a low concentration of epinephrine). Atrial EHT was significantly more sensitive to the drug (EC_{50} 23.3 nM vs. 195.4 nM in vEHT) and while aEHT completely ceased beating at concentrations higher than 100 nM, vEHT retained spontaneous activity even at the highest tested concentration. Moreover, under pacing and in the absence of epinephrine, we observed a direct negative inotropic effect in aEHT already at 0.3 μ M carbachol, whereas force of vEHT remained stable (Fig. 11b, c).

Discussion

In this study, we present a novel 3D model for the study of atrial biology in vitro and compared it to the well-established vEHT model, as well as native atrial and ventricular

heart muscle preparations. To our knowledge, this is the first description of a 3D model that allows for assessment of atrial contractility and drug response in a physiological multi-cell type context in vitro. Moreover, combined with optical pacing, drug-induced arrhythmia, or pro-fibrotic stimuli, the model may provide the basis for studying atrial fibrillation in vitro.

We based our protocol for the generation of aEHT on the EHT protocol by Hansen et al. [13]. While the process of EHT generation and culture as well as the range of possible scientific applications are similar, some technical differences were observed. Cell preparation from neonatal rat hearts yields \sim 5 vEHTs per heart, but only \sim 1 aEHT per heart. This diminishes one ethical advantage of EHT, to obtain several replicate experiments per heart. It retains all other advantages, such as the feasibility to test broad concentration ranges of unknown drugs, a high degree of standardization

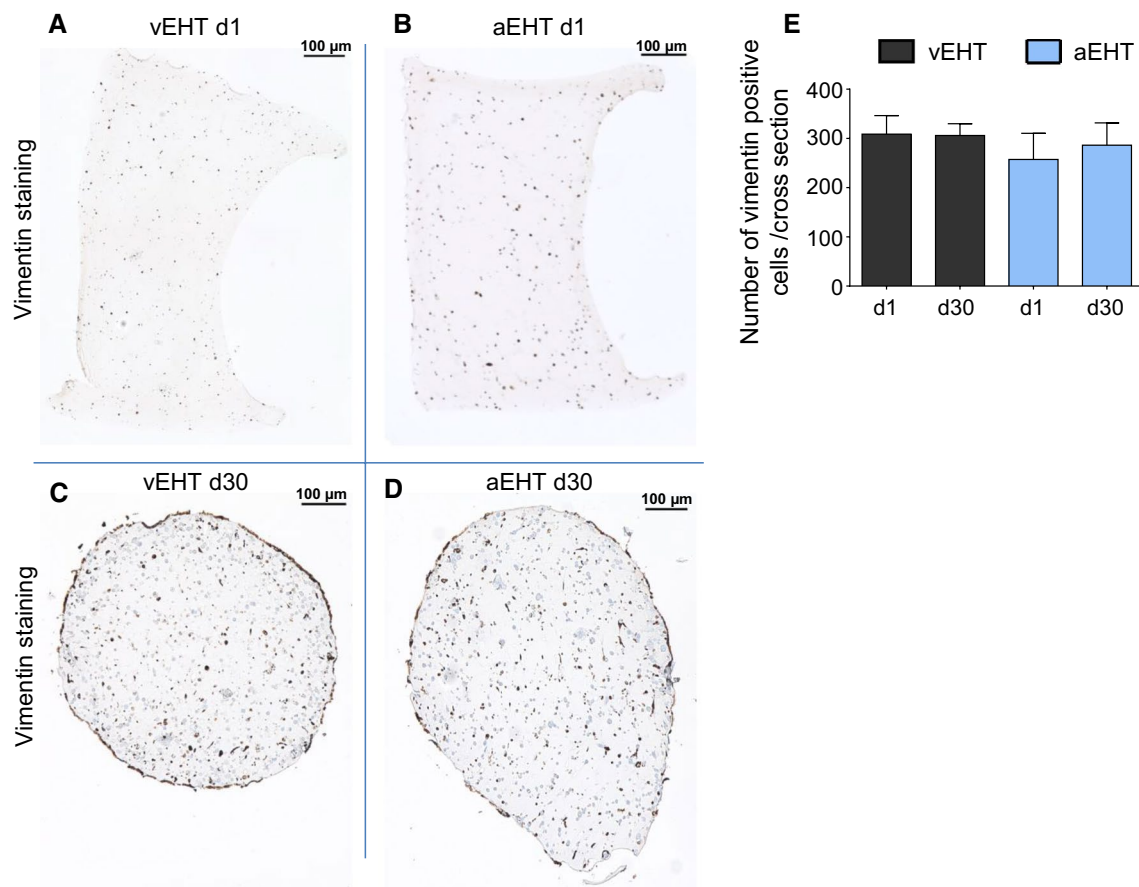


Fig. 10 EHT remodeling. Vimentin staining was performed in vEHT and aEHT paraffin sections on day 1 (**a, b**) and day 30 (**c, d**). The number of vimentin-positive cells per section was counted using ImageJ software (**e**). *n* = 3 for each condition

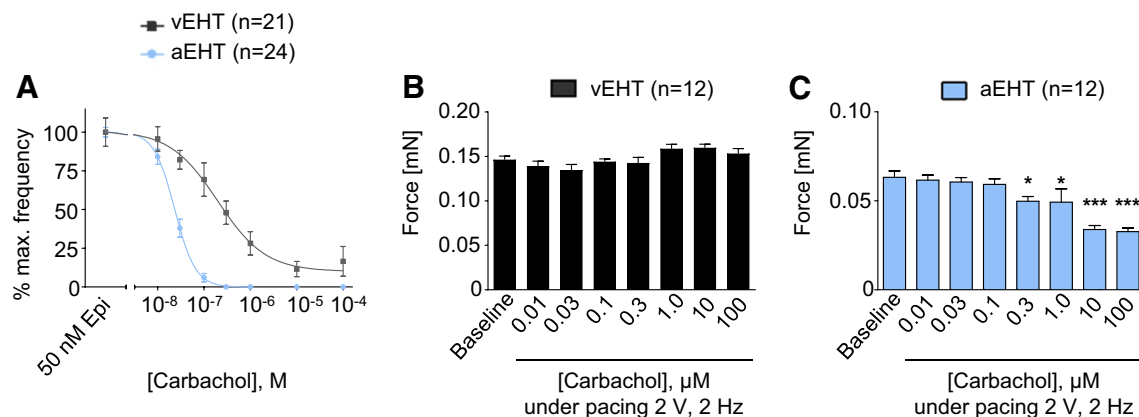


Fig. 11 Muscarinic stimulation by carbachol. **a** Carbachol concentration–response curves for spontaneous beating frequency of aEHT and vEHT in presence of 50 nM epinephrine (EC_{50} vEHT = 195.40 nM, EC_{50} aEHT = 23.31 nM). Normalized force generation of **b** vEHT

and **c** aEHT in the presence of different concentrations of carbachol and in the absence of epinephrine under bipolar electrical stimulation at 2 V, 4 ms pulse duration and 2 Hz; One-way ANOVA, Bonferroni post-test for multiple comparisons, **p* < 0.05, ****p* < 0.001

and reusability with stability for weeks [10]. Moreover, this aEHT protocol enables the simultaneous preparation of aEHT and vEHT, thus increasing the number of possible

experiments per killed animal. We did not observe obvious differences in handling, cell quality or reproducibility and found the same histological morphology in aEHT as in

vEHT (Fig. 9, Fig. S2). In summary, the robustness of the vEHT protocol was reflected in aEHT, underlined by the fact that we were able to generate seven aEHT batches without relevant batch-to-batch variation (Fig. S4, a through d).

When comparing aEHT directly to vEHT, the typical molecular and functional differences of atrial and ventricular tissue were reflected in our model. Contraction and relaxation time were shorter than in vEHT and contractile force was lower, representing the situation in cardiac tissue [27]. However, the most striking feature of aEHT was a slower and more regular beating pattern. Compared to vEHT, we assumed a higher number of cells with pacemaker activity in aEHT, as the sinoatrial nodes (SAN) were not removed during preparation. A high number of SAN cells leads to a higher probability of coincidental spontaneous action potential generations. Such a coincidence would be strong enough to activate the entire EHT and to override both the spontaneous activity of surrounding cardiomyocytes and their electrical sink properties [40] and thus induce regular beating. In vEHT with burst-like activity, only a few cells with slower pacemaker activity, such as His bundle and Purkinje fiber cells, are distributed across the tissue, explaining its periods of inactivity. While the high frequency during bursts in vEHT is counter-intuitive at first, it might well be explained by reentry, calcium storage overload during rest periods or various other, more complex mechanisms. Taking the above considerations into account, the lower frequency of aEHT (~60 bpm) compared to neonatal rat heart (~400 bpm) might be explained by the fact that individual isolated SAN myocytes beat at a slower rate than the intact heart [25]. As several SAN cells need to depolarize synchronously and summarize their action potential to activate the whole EHT, the likelihood for this event is decreasing with decreasing numbers and increasing distance of pacemaker cells. Both hold true for aEHT in which some nodal cells are lost during cell preparation and the remaining are distributed in a higher volume than in vivo. To confirm the presence of SAN cells, we measured the expression of two marker genes for pacemaker cells (*Shox2* and *Thy1*) and indeed found a significantly higher expression in aEHT.

The APD in aEHT was shorter than in vEHT again reflecting the situation in vivo. To evaluate possible functional implications of the APD, we performed force–frequency relationship (FFR) analysis by electrical stimulation with increasing frequencies. We observed an overall negative FFR in both EHT models, which is in line with the literature. Rodent myocardium usually displays a negative FFR in contrast to the positive FFR observed in larger mammals, such as human or dog [12, 26, 35]. However, this decline of force started at a higher pacing frequency in aEHT (3 Hz vs. 2 Hz in vEHT). Furthermore, aEHT followed the pacing pulses up to the maximum pacing frequency (10 Hz) while vEHT started losing capture at 7.5 Hz. To compensate

for increasing frequencies, ventricular tissue needs to accelerate its relaxation to ensure sufficient time for refilling of the ventricle FDAR which was observed in vEHT [37] but not in aEHT. This observation from aEHT is in line with data from Grimm et al. who observed constant, already maximally fast relaxation time in mouse atrial tissue [12]. One possible explanation for this observation might be the role of phospholamban (PLN) in FDAR in ventricular myocytes. Increasing stimulation rates were shown to disrupt the interaction between phospholamban and the sarcoplasmic calcium ATPase SERCA2a, leading to an accelerated sarcoplasmic reticulum Ca^{2+} uptake and to relaxation acceleration [37]. Indeed, our expression analysis exhibited a significantly lower *Pln* expression in aEHT compared to vEHT, which might explain the high basal SERCA2a activity and high according relaxation velocity, and the lack of FDAR in our atrial model.

For further electrophysiological characterization and to answer the question whether aEHT can complement the existing vEHT model as a drug screening platform, we treated both EHT models with the atrial-selective cholinomimetic drug carbachol. Carbachol activates the cardiac muscarinic M_2 receptor ($M_2\text{AChR}$), which indirectly regulates ion channel activity [14]. One important target is the inward rectifying potassium channel Kir3, which is primarily expressed in the SAN and in atrial tissue and is responsible for the acetylcholine-dependent repolarizing current I_{KACH} . Thus, I_{KACH} activation leads to APD shortening and decreased contractile force in the atrium and reduced spontaneous heart rate by hyperpolarization and delayed spontaneous depolarization in SAN [41]. Accordingly, carbachol (in the absence of adrenergic stimulation) exerted a physiological concentration-dependent negative inotropic effect in aEHT, but not in vEHT. The potency of CCh to evoke negative inotropy in aEHT is in line with that measured in murine atria (EC_{50} 0.4 μM) or the indirect negative inotropic effect in murine papillary muscles pretreated with isoprenaline (EC_{50} 0.4 μM [38]). With increasing drug concentrations, beating frequency decreased in both models. However, aEHT was much more sensitive to carbachol than vEHT and lost macroscopic beating activity at 300 nM. The observation of an effect on frequency in vEHT could be explained by the contribution of pacemaker cells from the AV node and bundle of His to spontaneous beating [19]. The canonical response to carbachol further supports the validity of our atrial in vitro model.

A notable difference between EHTs and their respective native heart correlate was the absolute APD, which was higher in both EHT models compared to adult tissue. A possible explanation is bradycardia-induced AP prolongation. Qi et al. demonstrated AP prolongation and ion current remodeling in the rabbit heart after 1–2 weeks of AV block-induced ventricular bradycardia [29]. Conversely,

APD decreases with increasing beating frequencies [4, 11]. Therefore, the constantly low spontaneous frequency of EHT might lead to the observed prolonged APD, which is in line with the observed higher *Cacnalc* expression after 30 days in EHT culture. Different developmental age could provide another explanation for the observed differences between adult tissue and EHT prepared from neonatal cells [16]. Lastly, the 3D cultivation format does not completely reflect tissue organization in vivo, which might affect the cell characteristics.

Limitations

The current study was performed with atrial cells from neonatal rats. Thus, the well-known disadvantages associated with rodents apply. Moreover, the removal of the SAN from the atria was not feasible for practical reasons, which leads to a possible bias due to the included pacemaker cells in the EHTs. However, the high reproducibility of the various batches of aEHT suggests a minor influence of those cells on reproducibility. Recent protocols which may eventually overcome species limitations allow for the generation of human atrial or even nodal cardiomyocytes from human-induced pluripotent stem cells and tissue engineering with these cells (hiPSC [6, 7, 19]). These protocols principally allow for patient-specific disease modeling even by direct reprogramming [9, 24]. Yet, at present, structural and functional immaturity and contamination with ventricular-like cardiomyocytes [6, 7], as well as work load, complexity and cost have to be weighed against the species advantage. Rat aEHTs exhibit a more mature phenotype, which is exemplified by a quantitatively normal effect of carbachol on contractile force and frequency, while the effect on $I_{K_{ACh}}$ current was smaller in hiPSC atrial-like cardiomyocytes [6, 20]. Thus, while human cardiac tissue engineering represents a revolutionary new tool for disease modeling, rat aEHT may be, at present, better suited to test for the effects of atrial-specific drugs, for drug testing and physiological experiments in general, and could pave the way for human atrial tissue engineering for which it may serve as a benchmark.

Conclusions

Taken together, we established a novel in vitro 3D rat cell culture model to study atrial biology, which reflects atrial physiology in terms of contractile function, gene expression, histology, electrophysiology, and the response to the atrial-selective drug carbachol. Further analyses are needed to explain the observed beating pattern and APD differences to adult native tissue. Our results suggest that rat atrial EHT might be a useful tool for atrial drug screening

and to study atrial biology in vitro due to its simplicity and cost-effectiveness.

Acknowledgements The authors want to thank Klaus Söhren, June Uebeler, Thomas Schulze, Tim Hartmann, and Grit Höppner for expert technical assistance. We additionally thank Tobias Krause for help with electrophysiological characterization, Alexander Fischer for imaging, Kristin Hartmann at Mouse Pathology Core Facility in Hamburg for histological staining, the team at FACS-Sorting Core Facility in Hamburg for their service and help regarding flow cytometry, and the UKE Microscopy Imaging Facility.

Author contributions All authors participated in the design of the experiments. JK performed atrial cell isolation and EHT preparation. AL performed force frequency experiments and histology. JK and AL performed drug response experiments, gene expression analysis, and flow cytometry. Contractility was assessed by JK, AL and JS. JK and KS performed whole-mount immunostainings. All electrophysiological experiments were done by MDL, with help from Tobias Krause and TC. Rat contractility data was contributed by Klaus Söhren and TC. JK, AL, JS and TE wrote the manuscript.

Funding This work was supported by funding from the DZHK (German Centre for Cardiovascular Research), the German Ministry of Education and Research (BMBF) and the e:Med symAtrial consortium, a BMBF initiative.

Compliance with ethical standards

Ethical standards All animal work was conducted in accordance with the Guide for the Care and Use of Laboratory Animals as adopted by the United States National Institutes of Health (NIH publication No. 85-23, revised 1996). All animal work was approved by the local Animal Welfare Committee of the City of Hamburg, Germany (approval #08/14). The manuscript does not contain clinical studies or patient data.

Conflict of interest TE is cofounder of EHT Technologies GmbH Hamburg, which provides technical equipment for making and video-optical analysis of EHTs.

References

1. Amos GJ, Wettwer E, Metzger F, Li Q, Himmel HM, Ravens U (1996) Differences between outward currents of human atrial and subepicardial ventricular myocytes. *J Physiol* 491(1):31–50. <https://doi.org/10.1113/jphysiol.1996.sp021194>
2. Balouch M, Kolek MJ, Darbar D (2014) Improved understanding of the pathophysiology of atrial fibrillation through the lens of discrete pathological pathways. *Glob Cardiol Sci Pract* 5:24–36. <https://doi.org/10.5339/gcsp.2014.5>
3. Barth AS, Merk S, Arnoldi E, Zwermann L, Kloos P, Gebauer M, Steinmeyer K, Bleich M, Kääb S, Pfeufer A, Überfuhr P, Dugas M, Steinbeck G, Nabauer M (2005) Functional profiling of human atrial and ventricular gene expression. *Pflügers Arch Eur J Physiol* 450:201–208. <https://doi.org/10.1007/s00424-005-1404-8>
4. Burashnikov A, Antzelevitch C (2006) Late-phase 3 EAD. A unique mechanism contributing to initiation of atrial fibrillation. *Pacing Clin Electrophysiol* 29:290–295. <https://doi.org/10.1111/j.1540-8159.2006.00336.x>

5. Christ T, Galindo-Tovar A, Thoms M, Ravens U, Kaumann AJ (2009) Inotropy and L-type Ca²⁺ current, activated by β 1- and β 2-adrenoceptors, are differently controlled by phosphodiesterases 3 and 4 in rat heart. *Br J Pharmacol* 156:62–83. <https://doi.org/10.1111/j.1476-5381.2008.00015.x>
6. Cyganek L, Tiburcy M, Sekeres K, Gerstenberg K, Bohnenberger H, Lenz C, Henze S, Salinas MSG, Zimmermann W-H, Hasenfuss G, Guan K (2018) Deep phenotyping of human induced pluripotent stem cell—derived atrial and ventricular cardiomyocytes. *J Clin Invest*. <https://doi.org/10.1172/jci.insight.99941DS1>
7. Devalla HD, Schwach V, Ford JW, Milnes JT, El-Haou S, Jackson C, Gkatzis K, Elliott DA, de Sousa Chuva, Lopes SM, Mummery CL, Verkerk AO, Passier R (2015) Atrial-like cardiomyocytes from human pluripotent stem cells are a robust preclinical model for assessing atrial-selective pharmacology. *EMBO Mol Med* 7:394–410. <https://doi.org/10.15252/emmm.201404757>
8. Eder A, Vollert I, Hansen A, Eschenhagen T (2016) Human engineered heart tissue as a model system for drug testing. *Adv Drug Deliv Rev* 96:214–224. <https://doi.org/10.1016/j.addr.2015.05.010>
9. Ghiroldi A, Piccoli M, Ciconte G, Pappone C, Anastasia L (2017) Regenerating the human heart : direct reprogramming strategies and their current limitations. *Basic Res Cardiol* 112:1–14. <https://doi.org/10.1007/s00395-017-0655-9>
10. Godier-Furnémont AFG, Tiburcy M, Wagner E, Dewenter M, Lämmle S, El-Armouche A, Lehnart SE, Vunjak-Novakovic G, Zimmermann W-H (2015) Physiologic force-frequency in engineered heart muscle by electromechanical stimulation. *Biomaterials* 60:82–91. <https://doi.org/10.1016/j.biomaterials.2015.03.055>
11. Grandi E, Pandit SV, Voigt N, Workman AJ, Dobrev D, Jalife J, Bers DM (2011) Human atrial action potential and Ca²⁺ model: sinus rhythm and chronic atrial fibrillation. *Circ Res* 109:1055–1066. <https://doi.org/10.1161/CIRCRESAHA.111.253955>
12. Grimm M, El-Armouche A, Zhang R, Anderson ME, Eschenhagen T (2007) Reduced contractile response to α 1-adrenergic stimulation in atria from mice with chronic cardiac calmodulin kinase II inhibition. *J Mol Cell Cardiol* 42:643–652. <https://doi.org/10.1016/j.yjmcc.2006.12.010>
13. Hansen A, Eder A, Bönstrup M, Flato M, Mewe M, Schaaf S, Aksehirliglu B, Schwörer A, Uebeler J, Eschenhagen T (2010) Development of a drug screening platform based on engineered heart tissue. *Circ Res* 107:35–44. <https://doi.org/10.1161/CIRCRESAHA.109.211458>
14. Harvey RD, Belevych AE (2003) Muscarinic regulation of cardiac ion channels. *Br J Pharmacol* 139:1074–1084. <https://doi.org/10.1038/sj.bjp.0705338>
15. Heijman J, Dobrev D (2014) Rat engineered heart tissue: a novel tool in the safety pharmacology toolkit? *Basic Res Cardiol* 109:437. <https://doi.org/10.1007/s00395-014-0437-6>
16. Hirt MN, Boeddinghaus J, Mitchell A, Schaaf S, Boernchen C, Mueller C, Schulz H, Hubner N, Stenzig J, Stoehr A, Neuber C, Eder A, Luther PK, Hansen A, Eschenhagen T (2014) Functional improvement and maturation of rat and human engineered heart tissue by chronic electrical stimulation. *J Mol Cell Cardiol* 74:151–161. <https://doi.org/10.1016/j.yjmcc.2014.05.009>
17. Jackman CP, Carlson AL, Bursac N (2016) Dynamic culture yields engineered myocardium with near-adult functional output. *Biomaterials* 111:66–79. <https://doi.org/10.1016/j.biomaterials.2016.09.024>
18. Jungen C, Scherschel K, Eickholt C, Kuklik P, Klatt N, Bork N, Salzbrunn T, Alken F, Angendohr S, Klene C, Mester J, Klöcker N, Veldkamp MW, Schumacher U, Willems S, Nikolaev VO, Meyer C (2017) Disruption of cardiac cholinergic neurons enhances susceptibility to ventricular arrhythmias. *Nat Commun* 27:14155. <https://doi.org/10.1038/ncomms14155>
19. Kurian T, Ambrosi C, Hucker W, Fedorov VV, Efimov IR (2010) Anatomy and electrophysiology of the human AV node. *PACE Clin Electrophysiol* 33:754–762. <https://doi.org/10.1111/j.1540-8159.2010.02699.x>
20. Lee JH, Protze SI, Laksman Z, Backx PH, Keller GM (2017) Human pluripotent stem cell-derived atrial and ventricular cardiomyocytes develop from distinct mesoderm populations. *Cell Stem Cell* 21(179–194):e4. <https://doi.org/10.1016/j.stem.2017.07.003>
21. Lemoine MD, Krause T, Koivumäki JT, Prondzynski M, Schulze ML, Girdauskas E, Willems S, Hansen A, Christ TET (2018) Human iPSC-derived engineered heart tissue as a sensitive test system for QT prolongation and arrhythmic triggers. *Circ Arrhythmia Electrophysiol*. <https://doi.org/10.1161/CIRCEP.117.006035>
22. Lemoine MD, Mannhardt I, Breckwoldt K, Prondzynski M, Flenner F, Ulmer B, Hirt MN, Neuber C, Horváth A, Kloth B, Reichenspurner H, Willems S, Hansen A, Eschenhagen T, Christ T (2017) Human iPSC-derived cardiomyocytes cultured in 3D engineered heart tissue show physiological upstroke velocity and sodium current density. *Sci Rep* 7:5464. <https://doi.org/10.1038/s41598-017-05600-w>
23. Magnani JW, Rienstra M, Lin H, Sinner MF, Lubitz S, Mcmanus DD, Dupuis J, Ellinor PT, Benjamin EJ (2011) Atrial fibrillation: current knowledge and future directions in epidemiology and genomics. *Circulation* 124:1982–1993. <https://doi.org/10.1161/CIRCULATIONAHA.111.039677>
24. Malan D, Zhang M, Stallmeyer B, Mu J, Fleischmann BK, Philipp ES, Boris S (2016) Human iPSC cell model of type 3 long QT syndrome recapitulates drug-based phenotype correction. *Basic Res Cardiol*. <https://doi.org/10.1007/s00395-016-0530-0>
25. Mesirca P, Alig J, Torrente AG, Müller JC, Marger L, Rollin A, Marquilly C, Vincent A, Dubel S, Bidaud I, Fernandez A, Seniuk A, Engeland B, Singh J, Miquerol L, Ehmke H, Eschenhagen T, Nargeot J, Wickman K, Isbrandt D, Mangoni ME (2015) Cardiac arrhythmia induced by genetic silencing of “funny” (f) channels is rescued by GIRK4 inactivation. *Nat Commun* 5:4664. <https://doi.org/10.1038/ncomms5664>
26. Neumann T, Ravens U, Heusch G (1998) Characterization of excitation–contraction coupling in conscious dogs with pacing-induced heart failure. *Cardiovasc Res* 37(2):456–466
27. Ng SYSY, Wong CKCK, Tsang SYSY (2010) Differential gene expressions in atrial and ventricular myocytes: insights into the road of applying embryonic stem cell-derived cardiomyocytes for future therapies. *Am J Physiol Physiol* 299:C1234–C1249. <https://doi.org/10.1152/ajpcell.00402.2009>
28. Page RL, Tilsch TW, Connolly SJ, Schnell DJ, Marcello SR, Wilkinson WE, Pritchett ELC (2003) Asymptomatic or “silent” atrial fibrillation frequency in untreated patients and patients receiving azimilide. *Circulation* 107:1141–1145. <https://doi.org/10.1161/01.CIR.0000051455.44919.73>
29. Qi XY, Yeh YH, Chartier D, Xiao L, Tsuji Y, Brundel BJJM, Kodama I, Nattel S (2009) The calcium/calmodulin/kinase system and arrhythmogenic after depolarizations in bradycardia-related acquired long-QT syndrome. *Circ Arrhythmia Electrophysiol* 2:295–304. <https://doi.org/10.1161/CIRCEP.108.815654>
30. Schneider CA, Rasband WS, Eliceiri KW (2012) NIH Image to ImageJ: 25 years of image analysis. *Nat Methods* 9:671–675. <https://doi.org/10.1038/nmeth.2089>
31. Schotten U, Verheule S, Kirchhof P, Goette A (2011) Pathophysiological mechanisms of atrial fibrillation: a translational appraisal. *Physiol Rev* 91:265–325. <https://doi.org/10.1152/physrev.00031.2009>
32. Smyrniak I, Mair W, Harzheim D, Walker SA, Roderick HL, Bootman MD (2010) Cell Calcium Comparison of the T-tubule system in adult rat ventricular and atrial myocytes, and its role in excitation–contraction coupling and inotropic stimulation. *Cell Calcium* 47:210–223. <https://doi.org/10.1016/j.ceca.2009.10.001>

33. Staerk L, Sherer JA, Ko D, Benjamin EJ, Helm RH (2017) Atrial fibrillation. *Circ Res* 120:1501–1517. <https://doi.org/10.1161/CIRCRESAHA.117.309732>
34. Stoehr A, Neuber C, Baldauf C, Vollert I, Friedrich FW, Flenner F, Carrier L, Eder A, Schaaf S, Hirt MN, Aksehirlioglu B, Tong CW, Moretti A, Eschenhagen T, Hansen A (2014) Automated analysis of contractile force and Ca²⁺ transients in engineered heart tissue. *AJP Heart Circ Physiol* 306:H1353–H1363. <https://doi.org/10.1152/ajpheart.00705.2013>
35. Szigligeti P, Pankucsi C, Bányász T, Varró A, Nánási PP (1996) Action potential duration and force-frequency relationship in isolated rabbit, guinea pig and rat cardiac muscle. *J Comp Physiol B* 166:150–155
36. Trayanova NA, Boyle PM, Arevalo HJ, Zahid S (2014) Exploring susceptibility to atrial and ventricular arrhythmias resulting from remodeling of the passive electrical properties in the heart: a simulation approach. *Front Physiol* 5:1–12. <https://doi.org/10.3389/fphys.2014.00435>
37. Valverde CA, Mundiña-Weilenmann C, Said M, Ferrero P, Vittoni L, Salas M, Palomeque J, Petroff MV, Mattiazzi A (2005) Frequency-dependent acceleration of relaxation in mammalian heart: a property not relying on phospholamban and SERCA2a phosphorylation. *J Physiol* 562:801–813. <https://doi.org/10.1113/jphysiol.2004.075432>
38. Vandecasteele G, Eschenhagen T, Scholz H, Stein B, Verde I, Fischmeister R (1999) Muscarinic and beta-adrenergic regulation of heart rate, force of contraction and calcium current is preserved in mice lacking endothelial nitric oxide synthase. *Nat Med* 5:331–334. <https://doi.org/10.1038/6553>
39. Weinberger F, Mannhardt I, Eschenhagen T (2017) Engineering cardiac muscle tissue. *Circ Res* 120:1487–1500. <https://doi.org/10.1161/CIRCRESAHA.117.310738>
40. Xie Y, Sato D, Garfinkel A, Qu Z, Weiss JN (2010) So little source, so much sink: requirements for after depolarizations to propagate in tissue. *Biophys J* 99:1408–1415. <https://doi.org/10.1016/j.bpj.2010.06.042>
41. Yeh YH, Lemola K, Nattel S (2007) Vagal atrial fibrillation. *Acta Cardiol Sin* 23:1–12. <https://doi.org/10.1161/CIRCULATIONAHA.107.737023>